Connecting hollow-core and standard single-mode fibers with perfect mode-field size adaptation

Ailing Zhong, Eric Numkam Fokoua, Meng Ding, Daniel Dousek, Dmytro Suslov, Stanislav Zvánovec, Francesco Poletti, Radan Slavík, and Matěj Komanec

***Abstract*—We propose an approach to interconnect a hollow-core fiber (HCF) of arbitrary core size with standard single-mode fiber with perfect mode-field size adaptation and experimentally achieve for the first time insertion loss agreeing with that predicted by simulations. We demonstrate this using three low-loss HCFs, including 1st window nested antiresonant nodeless fiber (NANF), 2nd window NANF and the state-of-the-art double NANF (DNANF). The connection with a minimum achieved insertion loss of 0.079 dB was permanently secured via gluing and did not degrade during 4 weeks of continuous measurement. To the best of our knowledge, this is the lowest reported value and is comparable to or lower than the connection between dissimilar single-mode fibers (e.g., standard single-mode fiber and dispersion-compensating fiber). We also show that such connection leads to excellent suppression of higher-order modes coupling, of importance to all applications sensitive to multi-path interference. Importantly, obtaining agreement between simulations and experiments validates for the first time the accuracy of the simulations and opens the door to further optimization via simulations with the ability to subsequently achieve the same result experimentally.**

***Index Terms*—Hollow-core fiber, nested antiresonant nodeless fiber, fiber interconnection, mode-field adaptation, higher-order mode, low-loss coupling.**

I. Introduction

Hollow-core optical fibers (HCFs) have progressed tremendously over the past decade. Their attenuation today is lower than that achievable in standard single-mode fibers (SSMFs) at all wavelengths except for the 1550 nm region, where the reported value of < 0.174 dB/km [1] achieved in a double nested antiresonant nodeless fiber (DNANF) geometry, is in parity with SSMFs. Additionally, these fibers possess exceptional polarization purity [2], low nonlinearity [3], broad transmission bandwidth [4], thermal insensitivity [5], etc. HCFs have thus found applications not only in fiber-optic communication, but also for high-power laser delivery [6], interferometry [7], gas sensing [8], and gas lasers [9].

With the demonstrated low attenuation levels in HCFs, a low-loss interconnection of HCF into SSMF-based systems is of particular importance. When short lengths of low-loss HCFs are used (*e.g.*, < 1 km), the HCF-SSMF coupling loss may become a dominant contributor to the total loss and thus reducing it may directly translate into reducing the overall loss. In applications where high optical power is transmitted, this loss may lead to overheating and thus lowering the damage threshold. Non-optimized HCF-SSMF interconnection may also lead to undesired coupling into higher-order modes (HOMs) of the HCF and subsequent multi-path interference. This requires attention, especially in applications in which shorter HCF lengths are used (*e.g.*, up to tens of meters), where light propagating via HOMs can still be present at the output despite their relatively high loss (*e.g.*, > 2000 dB/km in optimized designs [10]). Such multi-path interference is undesirable in most applications and, for example, in sensors may pose a limitation to the achievable resolution.

Theoretical limits of coupling between the fundamental mode of nested antiresonant nodeless (NANF) geometry of HCF and a Gaussian beam input (which well-approximates electromagnetic field profile at the output of a weakly-guiding SSMF) have been studied recently [11]. It was found that the minimum achievable loss depends on the order of the antiresonance window in which the HCF operates. For example, for a 6-tube design, the minimum loss was calculated to be 0.125 dB and 0.074 dB when operating in the 1st and 2nd antiresonance window, respectively. These numbers indeed depend slightly on the design, *e.g.*, the number of tubes, or the gaps between the tubes, which slightly alter the mode-field shape. We refer to this loss as limited by the "mode-field shape mismatch" between the SSMF and HCF. Several reports compared the finite-element simulated results with the best-achieved experimentally when coupling from free space (0.22 dB in [12]) and from SSMF (0.15 dB in [13]). However, the best-achieved experimental results were, at best, about twice as large as those predicted by simulations (0.074 dB [11]). Thus, experimental validation of simulations is so far missing.

Three main interconnection aspects must be considered in practice when targeting high-performance, ultra-low loss (limited by the mode-field shape mismatch) interconnection. Firstly, the mode-field sizes should be matched between the SSMF and HCF. Secondly, the Fresnel reflection (causing ~ 0.16 dB transmission loss) at the glass-air SSMF-HCF interface should be suppressed. Thirdly, the connection should be sealable to avoid ingress/egress of gas and subsequent degradation of the HCF endface [14], [15]. Below, we elaborate on these three aspects.

The mode-field diameter (MFD) of the mode exiting SSMF

Corresponding author: Ailing Zhong (zhongail@fel.cvut.cz).

Ailing Zhong, Daniel Dousek, Stanislav Zvánovec and Matěj Komanec are with Faculty of Electrical Engineering, Czech Technical University in Prague, 166 27 Prague, Czech Republic.

Meng Ding, Francesco Poletti and Radan Slavík are with Optoelectronic Research Centre, University of Southampton, SO17 1BJ, UK.

Eric Numkam Fokoua was with Optoelectronic Research Centre, University of Southampton, SO17 1BJ, UK and Dmytro Suslov was with Faculty of Electrical Engineering, Czech Technical University in Prague, 166 27 Prague, Czech Republic. Now they are with Microsoft, UK.

(typically 5-20 µm, depending on the fiber type and operating wavelength) must be matched to the MFD of the HCF fundamental mode. Typically the MFD of a HCF is 70% of the core size [11], therefore the MFD ranges from 10 µm through ∼22 µm for current low-loss DNANFs [1], 22-28 µm for current NANFs, to >40 µm for high power delivery [16] and HCF gas photonics [17]. An optimum method of this MFD adaptation should be fiber-compatible and enable accurate tuning of the MFD to the designed value. It should also provide a flat phase profile across the beam cross section (such as obtained in a Gaussian mode in its focus/waist), as the HCF fundamental guided mode has also a flat phase profile in the core region. Fiber-compatible mode-field adaptation using SSMF tapering [18], SSMF thermally-expanded core [13], reverse tapering [19], and splicing of a short segment of a graded index (GRIN) fiber [13] have been proposed. The last-mentioned method requires specific GRIN parameters to achieve the desired MFD with the required flat phase profile. The other methods can be directly customized in this regard.

The Fresnel back-reflection can be suppressed by SSMF tapering [18], [20], deposition of anti-reflective (AR) coating [13], [21] and angle-cleaving [22]–[24]. Back-reflection suppression to -27 dB over 390 nm bandwidth (from 1260 nm to 1650 nm) was demonstrated through tapering [18], below -40 dB over 60 nm using AR coating [13], and below -40 dB using 2° angled interface [24]. The angled interface lowers the back reflection but does not reduce the insertion loss (IL), as the otherwise back-reflected light is deflected out of the waveguides and thus not collected by the HCF. However, this method was shown to be advantageous when combined with the AR coating, achieving -60 dB back-reflection over 400 nm bandwidth with most of the light transmitted rather than deflected, achieving low transmission loss [21].

In terms of sealable interconnection, traditional fiber splicing [18], [24], gluing developed for planar lightwave circuits pigtailing [13], [21], or passive alignment inside a connector [25] have been reported. Splicing is generally not compatible with tip tapering or AR coating. There has been a recent report of splicing of AR-coated SSMF to an HCF [18], however, the AR coating properties degraded during the process due to high temperature during splicing, resulting in modest ∼-28 dB back-reflection. Passive alignment in a connector [25] does not provide a sealed connection and its long-term stability has not been, to the best of our knowledge, reported in the literature. Such a study would also need to investigate HOM cross-coupling, which may occur as the HCF degrades or the fibers' alignment drifts.

Here, we present an approach to obtain a beam of a desired MFD with the required flat phase profile using a single GRIN fiber. Considering three commercially-available GRIN fibers with various core diameters and numerical apertures, mode-field adaptation to any value between 10 and ∼90 µm is achievable with an SSMF input (*e.g.*, G.652 or G.657). This range is sufficient for most practical HCFs reported.

This technique then enabled us to realize HCF-SSMF interconnection at levels predicted by simulations (within the measurement error of ±0.006 dB). We demonstrate this by interconnecting HCFs with different MFD ranging from 22 to 25 µm. We also show the simulation-predicted advantage of using 2nd window HCF in terms of IL, achieving record-low IL of 0.079 dB, which was maintained even after gluing the interconnection. Besides showing a record-low SSMF-HCF IL, these results also validate the simulation predictions for the first time.

The lowest-achieved loss is also accompanied by reduced coupling into HOMs, enabling us to report record-high mode purity when coupling from an SSMF to an HCF.

Finally, achieving such a good agreement between the predictions and experiments suggests further improvements are possible using HCFs designed with minimized mode-field shape mismatch with SSMF, e.g., by increasing the number of tubes [26].

II. Principle and Simulations

Our interconnection design is illustrated in Fig. 1. A GRIN fiber is used as a mode-field adapter (MFA) to accommodate the MFD mismatch between SSMF and HCFs. To prepare the MFA, the GRIN fiber is first fusion-spliced with the SSMF. Subsequently, it is polished to the desired length within the accuracy of our GRIN length measurement of ±3 µm. When the GRIN fiber is polished to 0.25 pitch length (shown in Fig. 1a), the output beam is collimated at its output, requiring placing HCF to the MFA output without any gap. Recently we investigated how the gap between GRIN and HCF could be created to enable the insertion of functional elements such as filters [27], [28]. We first used a GRIN that produced a larger MFD than that of HCF. Subsequently, we polished GRIN slightly longer than 0.25 pitch (*e.g.*, 0.29 pitch), which made the output beam to focus slightly after exiting the MFA, gradually reaching a focal point (beam with flat phase) at a distance (our gap). By designing the GRIN length, HCF-matching MFD with flat phase (focus) was obtained at a distance from the GRIN, enabling a low-loss connection with a gap. Here, we use the same configuration, but rather than optimizing/maximizing the gap distance, we target the desired MFD with the gap as a free parameter (see Fig. 1b and c). This gap may be a desired feature, *e.g.*, for gas sensing [29], however, it would not be compatible with permanent interconnection using fusion splicing that requires zero gap. Fortunately, for the glued interconnection targeted here, this requires only minor modification of the assembly process and as we demonstrate here, it enables stable interconnection.

To demonstrate the flexibility of obtaining a suitable coupling beam of any desired MFD, we used three HCFs with as different core sizes as available to us. They have core sizes of 35.6 µm (1st window NANF with 6 pairs of nested tubes), 32.8 µm (2nd window NANF with 6 rings [13]), and 31.2 µm (the state-of-the-art DNANF with 5 rings [1]). As these fibers are of different geometries and operate over two different antiresonance windows, a comparison of simulated and experimental data should allow us to validate the accuracy of our simulations in these different geometries. The scanning electron micrograph (SEM) images of the used HCFs are presented in Fig. 1(d-f).

We first estimated the MFDs of the fundamental modes of each HCF sample by multiplying 70% with the core size [11],

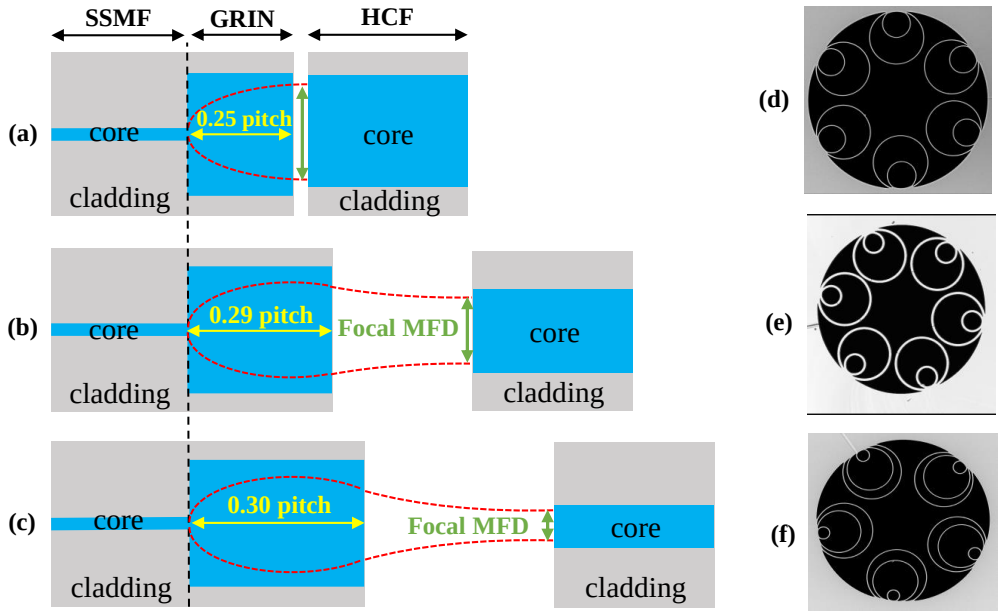

Fig. 1. Beam evolution (red dotted line) by virtue of (a) GRIN-based MFA at 0.25 pitch, (b) at 0.29 pitch, and (c) at 0.30 pitch. Scanning electron micrograph (SEM) images of (d) 1st window NANF, (e) 2nd window NANF, (f) 1st window DNANF.

obtaining 24.9 µm (1st window NANF), 22.9 µm (2nd window NANF [13]), and 21.8 µm (the-state-of-the-art DNANF [1]), respectively. Subsequently, we calculated the minimum IL between a perfectly matched circularly symmetric mode-field with Gaussian energy distribution to the calculated six/five-fold mode-field calculated using finite element simulations in Comsol Multiphysics using data from the end-faces of the particular (D)NANF [11], [13] at 1550 nm. We obtained values of 0.125 dB, 0.074 dB and 0.126 dB, for light coupling into 1st window NANF (in Fig. 1d), 2nd window NANF (in Fig. 1e) and 1st window DNANF (in Fig. 1f), respectively.

In the next step, we simulated light propagation from the SSMF, through the GRIN, followed by the free space. We used a finite-difference beam propagation technique implemented in Synopsys BeamPROP. For GRIN, we considered three selected commercially-available GRIN fibers with core diameters of 50, 100, and 200 µm. Their parameters are presented in Table I.

TABLE I
SPECIFICATIONS OF GRIN FIBERS.

GRIN fiber type	OM2	GRIN100	GRIN200
Core diameter (µm)	50	100	200
Cladding diameter (µm)	125	125	220
Numerical aperture	0.20	0.29	0.22

The focal MFD dependencies on GRIN length at 1550 nm are depicted in Fig. 2. The solid black curves illustrate how the focal MFD changes with respect to GRIN fiber length from 0.25 pitch (where the maximum MFD is obtained) to 0.50 pitch (where the MFD reduces to the same size as that of input SSMF). GRIN OM2-based MFA can provide focal MFD from 10 to ∼23 µm, GRIN100-based MFA then 10-32 µm, and GRIN200-based MFA 10-90 µm. The orange, blue, and yellow dashed lines represent the MFDs of fundamental modes of our 1st window NANF (24.9 µm), 2nd window NANF (22.9 µm) and DNANF (21.8 µm), respectively. As we can see in Fig. 2, the crossings between dashed lines (MFD of HCFs) and solid lines (focal MFDs of GRIN MFAs) indicate the optimum coupling into the specific HCF, which can be obtained by our MFAs of corresponding GRIN lengths.

Since GRIN100-based MFAs can provide optimum coupling into all three available HCFs (0.285 pitch for 24.9 µm, 0.295 pitch for 22.9 µm, and 0.301 pitch for 21.8 µm, respectively), we selected it for our demonstration. Subsequently, we fabricated a set of GRIN100-based MFAs with GRIN lengths close to/corresponding to the three different pitch lengths.

III. MEASUREMENT RESULTS

Figure. 3 presents the experimental setup we used for measuring the IL of the SSMF-MFA-HCF interconnection (denoted as a device under test - DUT). As we target measuring very low levels of IL, we took two precautions. Firstly, we measured two interfaces (SSMF-MFA-HCF-MFA-SSMF) to ensure we suppress the contribution from the coupling into HOMs [13]. It also increases the accuracy of the measurement, since we measure two interconnections, obtaining IL by dividing the measured loss (and thus also the measurement error) by two. Secondly, we paid particular attention to referencing our measurement, as we will describe later.

An erbium-doped fiber amplifier (EDFA) was used as a broadband light source, the light was then filtered to 1545-1555 nm via an optical band-pass filter (OBPF). Subsequently, the OBPF was connected with the DUT, which was followed by a 50/50 coupler, the outputs of the coupler were connected to a power meter (Thorlabs S154C) and an optical spectrum analyzer (OSA, Yokogawa AQ6375B), respectively.

In order to reference the IL measurement, we first spliced the OBPF output SSMF pigtail with the input SSMF pigtail

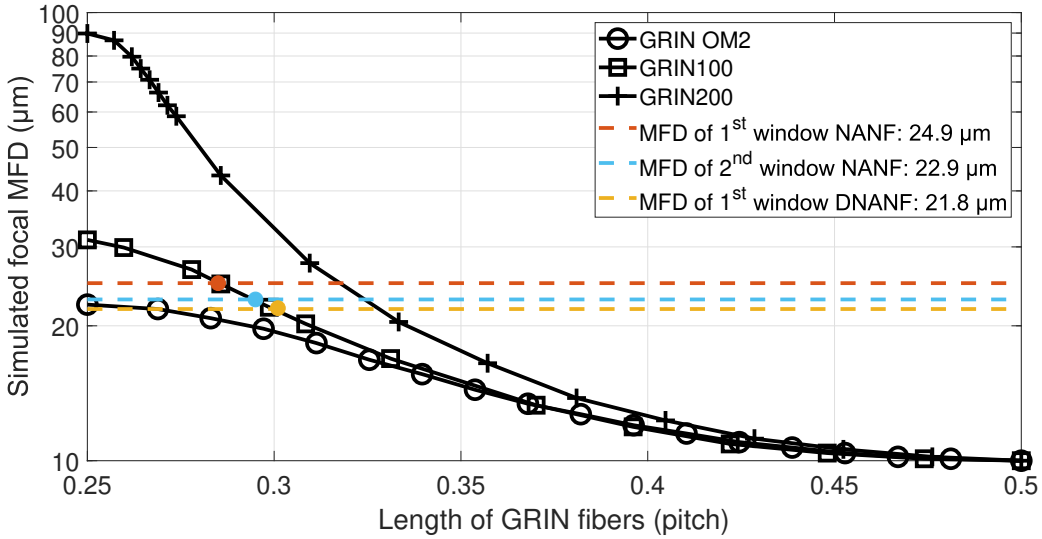

Fig. 2. Simulated dependence of focal MFD (plotted in logarithm scale) with respect to GRIN fiber length in pitch with predicted GRIN lengths for optimum coupling into particular HCFs.

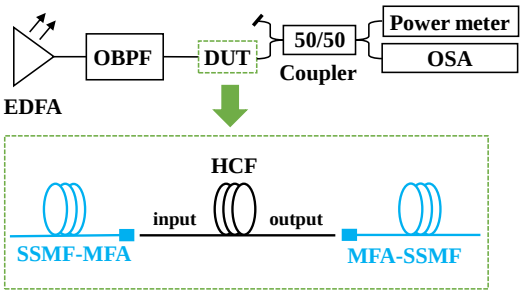

Fig. 3. Experimental setup for measuring the IL of the SSMF-MFA-HCF interconnection. (EDFA: erbium-doped fiber amplifier, OBPF: optical band-pass filter, DUT: device under test, OSA: optical spectrum analyzer, MFA: mode-field adapter, HCF: hollow-core fiber, SSMF: standard single-mode fiber).

of the 50/50 coupler and used this value at the power meter as a reference. In the next step, we cut this splice and spliced the DUT into the setup (two splices: at the input and output) with two identical GRIN100 MFAs at the input and output sides. The IL of each interconnection was calculated as the measured loss minus the HCF propagation loss, then divided by two. The SSMF-SSMF splice loss was neglected, as we usually obtain splice loss below the resolution of our power meter of 0.01 dB. This may result in overestimating the measured single SSMF-HCF connection loss by up to 0.005 dB. The fiber lengths of 1st window NANF, 2nd window NANF, and DNANF were 3 m, 8 m, and 3 m, respectively. The two 1st window HCFs had attenuation below 0.8 dB/km, making the propagation loss in the used 3 m sample of < 0.002 dB, which we neglected. As we expected IL for the 2nd window NANF coupled to the SSMF to be the lowest ever-measured (predicted at 0.074 dB), particular care was given to measure its loss. We measured directly the sample used in our demonstration using the very accurate Fabry-Perot method published in [30]. In this method, fiber under test is placed inside a high-finesse Fabry-Perot etalon in which light goes hundreds to thousands of times through the same fiber (> 1 km propagation length), enabling very accurate measurement of its attenuation. We measured the propagation loss in the 8 m-long HCF sample to be (0.022 ± 0.002) dB, which corresponds to attenuation of 1.8 dB/km).

We measured IL using our three HCF samples and four pairs of MFAs with different GRIN100 lengths, all with 4-layer Ta_2O_5/SiO_2 AR coating to avoid loss due to Fresnel back-reflection. Figure. 4(a-c) present the measured HCF-SSMF interconnection ILs (scatters) together with simulated ones (solid curve). The red dashed line marks the minimum calculated achievable IL when considering circularly-symmetric input field with Gaussian distribution [11], [13] at 1550 nm. For all three HCFs, we see reasonable agreement between the measured and simulated values, in particular, the measured minimum IL agrees well with the simulations (results are summarized in Table II). To evaluate this in detail, we first need to analyze the error of our measurement.

The largest error comes from our power meter, which has a minimum step of 0.01 dB. We consider in our analysis the power reading error of ± 0.01 dB in the measured power. Other sources of error are fiber loss (up to 0.002 dB, as discussed earlier) and splicing loss. We have spliced the SSMF-pigtailed 2nd window NANF several times, measuring loss periodically over a duration of 4 weeks and always achieving identical readings (of 0.18 dB). Thus, we neglect it here. Consequently, the total error of our measurement should be within $(\pm 0.01 + \pm 0.002 = \pm 0.012)$ dB. As this error is for two SSMF-HCF interconnections, we obtain IL error of ± 0.006 dB.

As concluded in Table II, the simulated GRIN100 lengths for optimum coupling agree well with those obtained experimentally. In terms of achieved IL, the measured values agree with the simulated ones within the measurement error (of

TABLE II
SIMULATED AND MEASURED OPTIMUM GRIN LENGTH AND ILS FOR SELECTED HCFS.

	NANF (1^{st} window)	NANF (2^{nd} window)	DNANF (1^{st} window)
Simulated optimum length of GRIN100 (pitch)	0.285	0.295	0.301
Measured optimum length of GRIN100 (pitch)	0.286	0.292	0.302
Theoretical loss of Gaussian mode coupling (dB)	0.125	0.074	0.126
Measured loss (dB)	0.120	0.079	0.120
Error (dB)	± 0.006	± 0.006	± 0.006

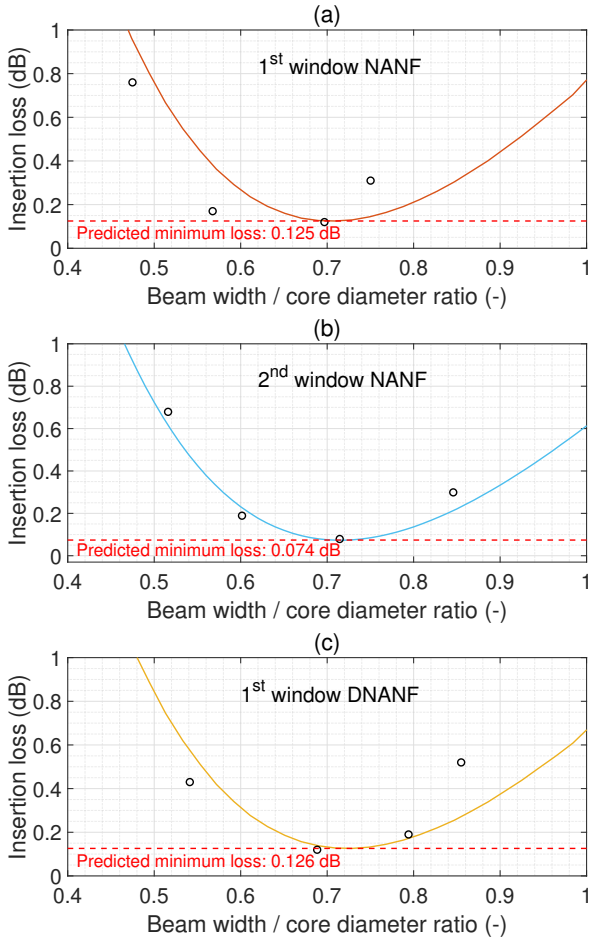

Fig. 4. Measured (scatters) and simulated (solid lines) IL for (a) 1^{st} window NANF, (b) 2^{nd} window NANF, and (c) 1^{st} window DNANF. Red dashed line: minimum calculated IL.

± 0.006 dB). We note that the measured IL values for the 1^{st} window HCFs are slightly below these simulated values, while it is the opposite for the 2^{nd} window NANF. This effect may be worth investigating further, but it would require a better power resolution/accuracy than available to us.

Importantly, our results verify the numerical accuracy of the simulations and also the accuracy of the theoretical model. It also shows the possibility of reaching simulation-predicted ILs in a real-case configuration.

We also measured the HOMs content in the 2^{nd} window NANF with our best-performing GRIN100-based MFA pair and compared it with the previously-demonstrated OM2-based MFAs published in [13] that used HCF from the same draw band. We used the same method as illustrated in [13] with the setup presented in Fig. 3. The results are shown in Fig. 5 with a comparison of previously-achieved results using OM2-based MFA in [13]. We can see that there are two predominantly-excited HOMs, LP_{11} mode and LP_{02} mode, which are highlighted in green and red color, respectively. LP_{11} mode excitation originates from the slight asymmetry of the fabricated NANF [13] rather than MFA itself. Thus, we would expect the same value of cross-coupling into the LP_{11} mode here and in previous work, which is confirmed in Fig. 5(a) and (b). As for LP_{02} mode cross-coupling, we observe a substantial reduction in our current work, which is consistent with better mode-matching of the input field with the fundamental mode of HCF, witnessed by its IL reduction from 0.15 dB in [13] to current 0.079 dB.

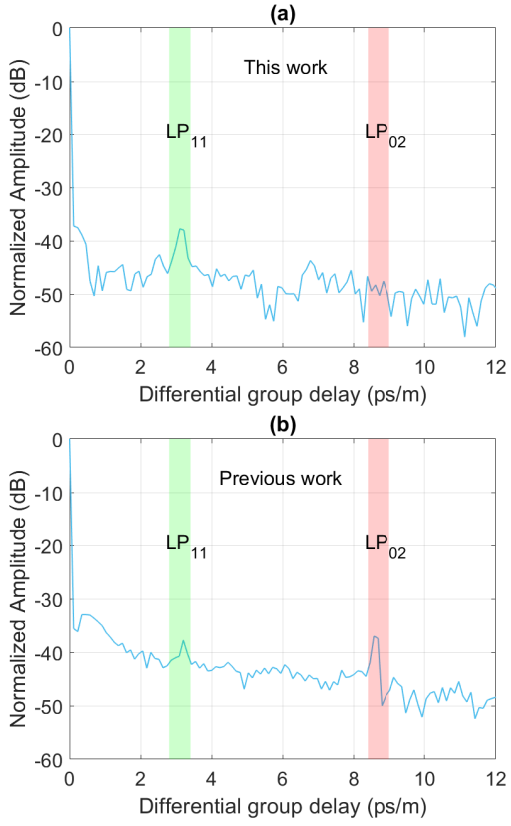

Fig. 5. Fourier transform of the transmission spectra in the 2^{nd} window NANF by the virtue of (a) GRIN100-based MFA (this work), (b) OM2-based MFA (previous work [13]).

We further analyzed our interconnection IL over a broad bandwidth of 1200 nm to 2000 nm by replacing the EDFA +

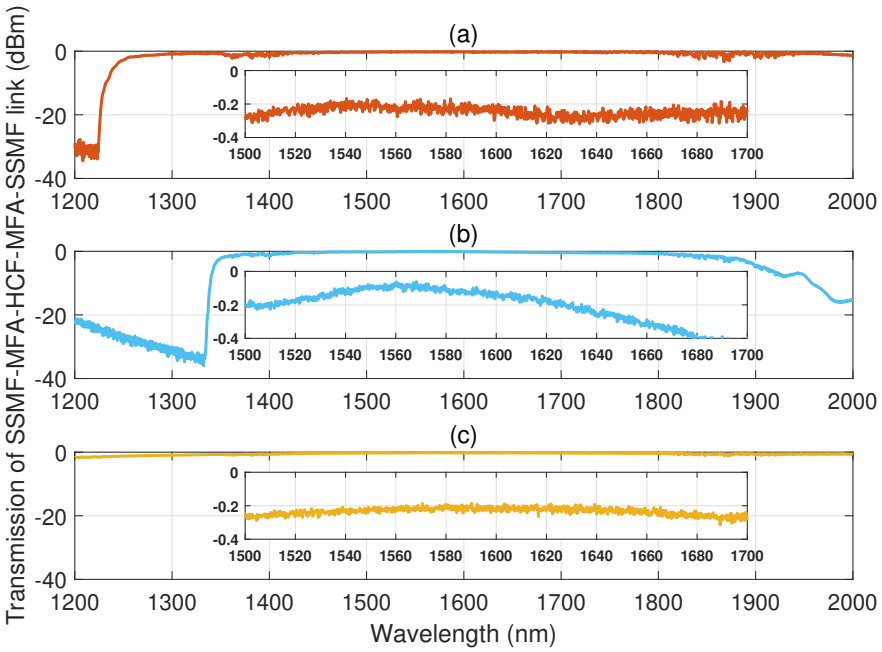

Fig. 6. Transmission spectrum in the link of SSMF-MFA-HCF-MFA-SSMF, using (a) 1st window NANF, (b) 2nd window NANF, and (c) 1st window DNANF. Insets: zoomed in spectrum in the wavelength range between 1500 nm and 1700 nm.

OBPF in Fig. 3 with a super-continuum source (NKT EXR-15). We first connected the super-continuum source output with the input of the 50/50 coupler and recorded the spectrum on OSA as a reference. Subsequently, we spliced DUT into the setup, obtaining spectral transmission loss of the SSMF-MFA-HCF-MFA-SSMF link. Figure. 6 presents the transmission spectra with 1st window NANF, 2nd window NANF and DNANF, respectively. The insets illustrate the transmission loss in detail across the wavelength range of 1500-1700 nm.

In Fig. 6 (a) we see that the 1st window NANF transmission window starts around 1230 nm. In the region of 1500–1700 nm, the transmission has a flat trend with slow fluctuation of only $\sim$0.1 dB and fast fluctuations (usually present due to multi-path interference with HOM) well below this value. In Fig. 6 (b), the 2nd window NANF shows, as expected for the 2nd window, a narrower transmission window. In the region of 1500–1700 nm, it shows a power variation of $\sim$0.3 dB, again with fast fluctuations well below this. Figure. 6 (c) demonstrates the transmission spectra in DNANF, which has the broadest transmission bandwidth among these three HCFs. The transmission spectrum (1500 nm–1700 nm) has a similar fluctuation ($\sim$0.06 dB) as in the 1st window NANF, again with negligible fast fluctuations, showing excellent HOM suppression.

IV. Permanent Interconnection

Here, we demonstrate a permanent interconnection using the gluing technique described in [29], with its long-term stability and performance over a range of temperatures shown in [31]. To accommodate the slight gap between the MFA and HCF, we used glue with high viscosity. We glued the lowest-loss sample (using 2nd window NANF) and obtained record-low-loss permanently connected SSMF-HCF-SSMF interconnection.

The measured loss prior to gluing was 0.18 dB (0.079 dB for each of the two interconnections plus 0.022 dB for the fiber propagation loss). This increased by 0.01 dB when gluing one side, but this relaxed back to 0.18 dB when removed from the holder. The situation on the other side was similar. We re-measured the sample periodically for 4 weeks, splicing it into the setup (to allow for power calibration), always measuring a value of 0.18 dB, showing excellent stability as well as repeatability of our measurement.

Figure. 7 shows the SSMF-HCF-SSMF sample with 8-m HCF and both interconnections in a protective housing.

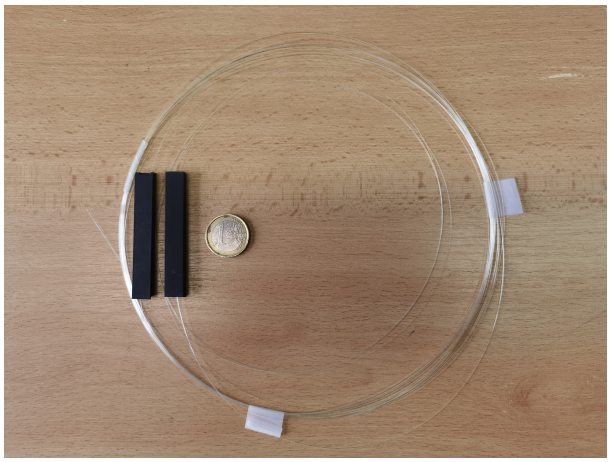

Fig. 7. Photograph of the permanently-interconnected 2nd window NANF with two SSMFs with an average SSMF-HCF IL of 0.079 dB.

V. Conclusions

We have demonstrated for the first time HCF-SSMF interconnection with IL that agrees perfectly with loss predicted by simulations within our measurement error of ± 0.006 dB. Besides achieving low connection loss, such a good agreement between the experimental results and simulations also validates high accuracy of the simulations. We made this comparison using NANF (core size of 35.6 µm) and DNANF (core size 31.2 µm) operating in the 1st window, obtaining IL (0.120 ± 0.006) dB for both of them. This agrees with the predicted minimum IL of 0.125 and 0.126 dB, respectively. Further, we tested it on the 2nd window NANF (core diameter of 32.8 µm), achieving record-low IL of (0.079 ± 0.006) dB) that also agrees with the simulated IL of 0.074 dB. We have achieved these results by designing a mode-field adaptation technique that enables arbitrary mode-field adaptation using commercially-available GRIN fibers. Besides achieving record-low IL for the respective (D)NANFs, our work validated for the first time the accuracy of the published numerical simulations.

Based on our simulations, our interconnection technique can adapt MFD in a wide continuous range of 10-90 µm using commercially-available GRIN fibers, which cover most HCF core diameters. We validated it experimentally, achieving predicted IL for a range of MFDs from 21.8 to 24.9 µm.

We have also characterized IL of the interconnection over a broad wavelength range, showing a variation of ~ 0.06 dB for SSMF-DNANF-SSMF over a 200 nm band (~ 0.03 dB for a single SSMF-DNANF interconnection).

Finally, we glued (permanently interconnected) the lowest-loss connection and observed no degradation (within the measurement error of ± 0.006 dB) over a 4-weeks period.

The demonstrated SSMF-DNANF connection with negligible HOM content and IL of 0.12 dB was achieved on DNANF design that holds the attenuation record of 0.174 dB/km. This brings HCF technology truly on par with SSMF systems.

Acknowledgement

This work was supported by the Czech Science Foundation (GACR) grant GA22-32180S and by the EPSRC projects EP/P030181/1 and EP/W037440/1.

Data availability

Data underlying the results presented in this paper will be available at the University of Southampton research repository (DOI: XXX.XXX.XXX).

Disclosures

The authors declare no conflicts of interest.

References

[1] G. T. Jasion, H. Sakr, J. R. Hayes, S. R. Sandoghchi, L. Hooper, E. N. Fokoua, A. Saljoghei, H. C. Mulvad, M. Alonso, A. Taranta *et al.*, "0.174 dB/km Hollow Core Double Nested Antiresonant Nodeless Fiber (DNANF)," in *2022 Optical Fiber Communications Conference and Exhibition (OFC)*. IEEE, 2022, pp. 1–3.

[2] A. Taranta, E. Numkam Fokoua, S. Abokhamis Mousavi, J. Hayes, T. Bradley, G. Jasion, and F. Poletti, "Exceptional polarization purity in antiresonant hollow-core optical fibres," *Nature Photonics*, vol. 14, no. 8, pp. 504–510, 2020.

[3] H. Sakr, Y. Hong, T. Bradley, G. Jasion, J. Hayes, H. Kim, I. Davidson, E. N. Fokoua, Y. Chen, K. Bottrill *et al.*, "Interband short reach data transmission in ultrawide bandwidth hollow core fiber," *Journal of Lightwave Technology*, vol. 38, no. 1, pp. 159–165, 2020.

[4] B. Debord, A. Amsanpally, M. Chafer, A. Baz, M. Maurel, J.-M. Blondy, E. Hugonnot, F. Scol, L. Vincetti, F. Gérôme *et al.*, "Ultralow transmission loss in inhibited-coupling guiding hollow fibers," *Optica*, vol. 4, no. 2, pp. 209–217, 2017.

[5] M. Ding, Z. Feng, D. Marpaung, X. Zhang, M. Komanec, D. Suslov, D. Dousek, S. Zvánovec, E. R. N. Fokoua, T. D. Bradley *et al.*, "Optical fiber delay lines in microwave photonics: Sensitivity to temperature and means to reduce it," *Journal of lightwave technology*, vol. 39, no. 8, pp. 2311–2318, 2021.

[6] H. Mulvad, S. Abokhamis Mousavi, V. Zuba, L. Xu, H. Sakr, T. Bradley, J. Hayes, G. Jasion, E. Numkam Fokoua, A. Taranta *et al.*, "Kilowatt-average-power single-mode laser light transmission over kilometre-scale hollow-core fibre," *Nature Photonics*, vol. 16, no. 6, pp. 448–453, 2022.

[7] B. Shi, G. Marra, Z. Feng, H. Sakr, J. R. Hayes, E. R. N. Fokoua, M. Ding, F. Poletti, D. J. Richardson, and R. Slavík, "Temperature insensitive delay-line fiber interferometer operating at room temperature," *Journal of Lightwave Technology*, vol. 40, no. 16, pp. 5716–5721, 2022.

[8] H. Bao, W. Jin, Y. Hong, H. L. Ho, S. Gao, and Y. Wang, "Phase-modulation-amplifying hollow-core fiber photothermal interferometry for ultrasensitive gas sensing," *Journal of Lightwave Technology*, vol. 40, no. 1, pp. 313–322, 2022.

[9] Z. Zhou, Z. Wang, W. Huang, Y. Cui, H. Li, M. Wang, X. Xi, S. Gao, and Y. Wang, "Towards high-power mid-IR light source tunable from 3.8 to 4.5 μm by HBr-filled hollow-core silica fibres," *Light: Science & Applications*, vol. 11, no. 1, p. 15, 2022.

[10] E. N. Fokoua, S. A. Mousavi, G. T. Jasion, D. J. Richardson, and F. Poletti, "Loss in hollow-core optical fibers: mechanisms, scaling rules, and limits," *Advances in Optics and Photonics*, vol. 15, no. 1, pp. 1–85, 2023.

[11] E. N. Fokoua, R. Slavik, D. J. Richardson, and F. Poletti, "Limits of coupling efficiency into hollow-core antiresonant fibers," in *CLEO: Science and Innovations*. Optica Publishing Group, 2021, pp. STu1Q–4.

[12] V. Zuba, H. C. H. Mulvad, R. Slavík, H. Sakr, F. Poletti, D. J. Richardson, and E. N. Fokoua, "Experimental Investigation into Optimum Laser Coupling Efficiency into Hollow-Core NANFs," in *2022 Conference on Lasers and Electro-Optics (CLEO)*. IEEE, 2022, pp. 1–2.

[13] D. Suslov, M. Komanec, E. R. N. Fokoua, D. Dousek, A. Zhong, S. Zvánovec, T. D. Bradley, F. Poletti, D. J. Richardson, and R. Slavík, "Low loss and high performance interconnection between standard single-mode fiber and antiresonant hollow-core fiber," *Scientific Reports*, vol. 11, no. 1, pp. 1–9, 2021.

[14] S. Rikimi, Y. Chen, T. D. Bradley, I. A. Davidson, H. Sakr, A. A. Taranta, K. Harrington, F. Poletti, M. N. Petrovich, D. J. Richardson *et al.*, "Comparison between the Optical Performance of Photonic Bandgap and Antiresonant Hollow Core Fibers after Long-Term Exposure to the Atmosphere," in *2022 Optical Fiber Communications Conference and Exhibition (OFC)*. IEEE, 2022, pp. 1–3.

[15] S. Rikimi, Y. Chen, T. W. Kelly, I. A. Davidson, G. T. Jasion, M. Partridge, K. Harrington, T. D. Bradley, A. A. Taranta, F. Poletti *et al.*, "Internal gas composition and pressure in as-drawn hollow core optical fibers," *Journal of Lightwave Technology*, vol. 40, no. 14, pp. 4776–4785, 2022.

[16] R. Safaei, G. Fan, O. Kwon, K. Légaré, P. Lassonde, B. E. Schmidt, H. Ibrahim, and F. Légaré, "High-energy multidimensional solitary states in hollow-core fibres," *Nature Photonics*, vol. 14, no. 12, pp. 733–739, 2020.

[17] F. Yang, F. Gyger, and L. Thévenaz, "Intense brillouin amplification in gas using hollow-core waveguides," *Nature photonics*, vol. 14, no. 11, pp. 700–708, 2020.

[18] C. Wang, R. Yu, C. Xiong, J. Zhu, and L. Xiao, "Ultralow-loss fusion splicing between antiresonant hollow-core fibers and antireflection-coated smfs with low return loss," *Optics Letters*, vol. 48, no. 5, pp. 1120–1123, 2023.

[19] C. Wang, R. Yu, B. Debord, F. Gérôme, F. Benabid, K. S. Chiang, and L. Xiao, "Ultralow-loss fusion splicing between negative curvature hollow-core fibers and conventional SMFs with a reverse-tapering method," *Optics Express*, vol. 29, no. 14, pp. 22 470–22 478, 2021.

[20] S. Xie, R. Pennetta, and P. S. J. Russell, "Self-alignment of glass fiber nanospike by optomechanical back-action in hollow-core photonic crystal fiber," *Optica*, vol. 3, no. 3, pp. 277–282, Mar 2016.

[21] D. Suslov, E. N. Fokoua, D. Dousek, A. Zhong, S. Zvánovec, T. D. Bradley, F. Poletti, D. J. Richardson, M. Komanec, and R. Slavík, "Low loss and broadband low back-reflection interconnection between a hollow-core and standard single-mode fiber," *Optics Express*, vol. 30, no. 20, pp. 37 006–37 014, 2022.

[22] G. A. Miller and G. A. Cranch, "Reduction of Intensity Noise in Hollow Core Optical Fiber Using Angle-Cleaved Splices," *IEEE Photonics Technology Letters*, vol. 28, no. 4, pp. 414–417, Feb 2016.

[23] F. Couny, F. Benabid, and P. S. Light, "Reduction of Fresnel Back-Reflection at Splice Interface Between Hollow Core PCF and Single-Mode Fiber," *IEEE Photonics Technology Letters*, vol. 19, no. 13, pp. 1020–1022, 2007.

[24] C. Zhang, E. N. Fokoua, S. Fu, M. Ding, F. Poletti, D. J. Richardson, and R. Slavík, "Angle-spliced smf to hollow core fiber connection with optimized back-reflection and insertion loss," *Journal of Lightwave Technology*, vol. 40, no. 19, pp. 6474–6479, 2022.

[25] Z. Zhang, A. Jia, Y. Hong, W. Ding, S. Gao, and Y. Wang, "Ultralow-loss, plug-and-play hollow-core fiber interconnection," in *2022 Optical Fiber Communications Conference and Exhibition (OFC)*. IEEE, 2022, pp. 1–3.

[26] V. Zuba, H. C. H. Mulvad, R. Slavík, H. Sakr, F. Poletti, D. J. Richardson, and E. N. Fokoua, "Limits of Coupling Efficiency into Hollow-core Antiresonant Fibres," *Journal of Lightwave Technology*, 2023.

[27] A. Zhong, D. Dousek, D. Suslov, S. Zvánovec, E. N. Fokoua, F. Poletti, D. J. Richardson, R. Slavík, and M. Komanec, "Hollow-core to standard fiber interconnection with customized air-gap distance," in *2022 Conference on Lasers and Electro-Optics (CLEO)*. IEEE, 2022, pp. 1–2.

[28] A. Zhong, M. Ding, D. Dousek, D. Suslov, S. Zvánovec, F. Poletti, D. J. Richardson, R. Slavík, and M. Komanec, "Gap design to enable functionalities into nested antiresonant nodeless fiber based systems," *Optics Express*, vol. 31, no. 9, pp. 15 035–15 044, 2023.

[29] D. Suslov, T. W. Kelly, S. Rikimi, A. Zhong, A. Taranta, S. Zvánovec, F. Poletti, D. J. Richardson, M. Komanec, N. Wheeler *et al.*, "Towards compact hollow-core fiber gas cells," in *2022 Conference on Lasers and Electro-Optics (CLEO)*. IEEE, 2022, pp. 1–2.

[30] M. Ding, E. R. N. Fokoua, T. D. Bradley, F. Poletti, D. J. Richardson, and R. Slavík, "Finesse limits in hollow core fiber based Fabry-Perot interferometers," *Journal of Lightwave Technology*, vol. 39, no. 13, pp. 4489–4495, 2021.

[31] D. Dousek, M. Komanec, A. Zhong, D. Suslov, S. Zvánovec, P. Veselỳ, Y. Chen, T. D. Bradley, E. R. N. Fokoua, F. Poletti *et al.*, "Long-term stability of hollow core to standard optical fiber interconnection," in *Micro-structured and Specialty Optical Fibres VII*, vol. 11773. SPIE, 2021, pp. 205–210.